Experimental Characterization of a Wire-Fed Metal-Propellant Hollow Cathode

Braden Oh*, Carter Krumins†, Trevor Jarvis‡, Tate M. Gill§, and Benjamin A. Jorns¶
University of Michigan, Ann Arbor MI, 48109

The performance of a barium oxide hollow cathode on zinc propellant is compared to performance on krypton propellant. Historical metal propellant feed systems relying on sublimation or boiling struggle with propellant metering and scalability for flight systems. This study demonstrates a wire-feed system for zinc delivery and measures anode current-voltage characteristics, plume Langmuir probe data, and oscillations in discharge current at 10 sccm and 15 sccm of zinc and krypton flow. It is found that anode coupling voltages are approximately 50% lower for zinc than for krypton and this is attributed to a lower resistivity of the plasma with zinc propellant. It is also found that the zinc plasma is more quiescent for the same operating conditions compared to operation with krypton. These findings ultimately show that the response of the cathode with zinc is not outside family for cathode operation on noble gases, providing a promising path forward for the option of this propellant for Hall thruster operation.

I. Introduction

Metal-propellant electric propulsion systems hold several key advantages for high power operation both on the ground and in space due to their condensability, high storage densities, and low costs. In orbit, metals such as bismuth and zinc store more densely than critical xenon [1] without requiring pressurization or cryogenic temperatures. On the ground, metals can be rapidly cryopumped on the walls of test facilities at ordinary temperatures, [2], reducing strain on facility pumps even at high flow rates and enabling ground testing at powers in excess of 100 kW.

Because of these advantages, metal propellant Hall thrusters have been the subject of previous development efforts directed toward high-power, ground-based testing. The TSNIIMASH D-140 thruster, for instance, reportedly demonstrated powers of 100-140 kW on bismuth, a nontoxic and high mass propellant option [3]. Bismuth was further explored at high specific impulses through the NASA VHITAL program [2–4], but efforts to develop a propellant feed system operable in microgravity were unsuccessful [5]. Bismuth exhibits extremely low vapor pressures, so must be heated to temperatures in excess of 800-1000°C to be flowed into a thruster. Further experiments performed by Busek Co. [6] and Michigan Technological University (MTU) [7] successfully demonstrated bismuth Hall thruster discharges, but both required the full mass of propellant to be liquefied in order to operate, relied on gravity, and neither actively controlled or metered the propellant flow rate.

An alternative metal propellant is zinc, which has been explored at Busek [8], MTU [9], and the University of Southampton (Soton) [10, 11]. Although being lighter than bismuth, zinc is nontoxic and exhibits substantial vapor pressures in the range 350-500°C, meaning it can be sublimated at modest flow rates before melting at 419°C. Soton and MTU delivered zinc propellant by sublimating zinc off a solid block either at the anode (MTU, [9]) or behind the anode, with the aid of a secondary heater (Soton, [10, 11]). However, neither Soton nor MTU were able to actively meter flow rate and MTU explicitly observed thermal runaway as propellant evaporation drove a positive feedback loop [9]. Busek delivered propellant to a Hall thruster by boiling zinc in a temperature-controlled liquid reservoir, thereby arresting thermal runaway at the costs of actively melting the entire propellant reservoir and gravity reliance [8]. Busek also reported vaporization data from a wire-fed sublimation system for zinc and magnesium, but did not disclose connecting this feed system to a thruster [8].

With these limitations in mind, a wire-fed delivery system could be a key enabler for flight-like metal propellant systems. It unlocks active propellant metering and arrests thermal runaway through precise control over the length of wire inserted into the thruster; it also enables storage scalability and heater power savings by only requiring the tip of

*Ph.D. Candidate, Department of Aerospace Engineering, Student Member AIAA
†Ph.D. Pre-Candidate, Department of Aerospace Engineering
‡Undergraduate researcher, Department of Aerospace Engineering
§Research scientist, Department of Aerospace Engineering, Member AIAA
¶Associate Professor, Department of Aerospace Engineering, Associate Fellow AIAA

the wire to be heated. This overcomes the challenges of propellant metering and scalability inherent to all previous heated-reservoir boiling/sublimation systems [2–11].

Although substantial efforts have been directed towards metal propellant thrusters, little work has been directed toward metal hollow cathode systems. Bismuth has reportedly been tested in lanthanum hexaboride (LaB_6) hollow cathodes by TSNIIMASH [2] and MTU [12, 13], but all aforementioned MTU, Busek, and Soton thrusters utilized xenon fueled hollow cathodes. Zinc, meanwhile, appears to be unexplored in the literature as a hollow cathode propellant. The need is therefore apparent for the development of a wire feed system for metal propellants and a quantitative investigation of the feasibility and performance of metal propellants in hollow cathodes.

In this paper, we develop a zinc wire-fed hollow cathode, measure its performance and plasma properties, and compare these metrics to operation on krypton. In Section II, we describe the hollow cathode design and detail the facility and diagnostic tools we employed. In Section III we present the results of testing this cathode on krypton and zinc. In Section IV we discuss the physical reasons for the differences between krypton and zinc operation.

II. Experimental Setup & Diagnostics

In this section we first describe the hollow cathode test article that we employed and then the modifications we made to our test facility to accommodate condensable propellant testing. We close by describing the diagnostic tools and techniques we employed in this study.

A. Test article

The device we used for testing was a barium oxide (BaO) hollow cathode that employed three stages of heaters to obtain zinc liquefaction and evaporation in a repeatable manner. A cross section of the assembled test article is shown in Fig. 1a.

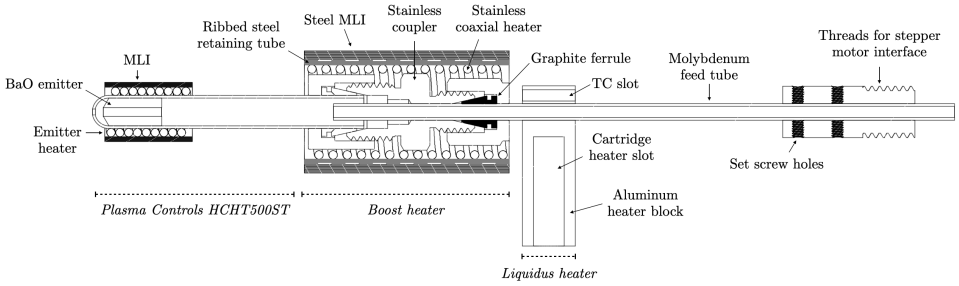

(a)

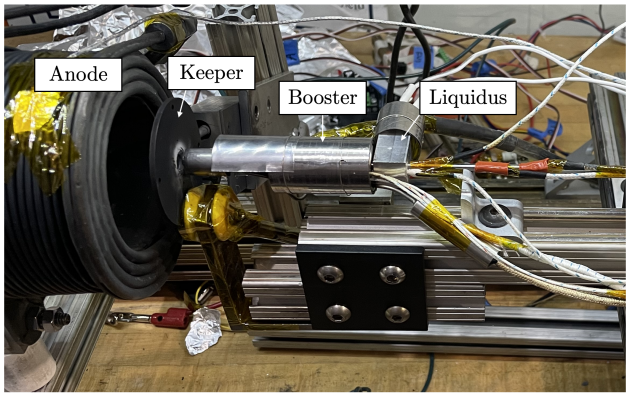

(b)

Fig. 1 a) Schematic and b) photographs of the cathode experimental configuration with wire-fed metal flow system.

The cathode tip assembly–comprising the emitter, emitter heater, and cathode tube–was a Plasma Controls HCHT500ST. The HCHT500ST contains a 1/4" swage interface which we connected to a 1/4-to-1/8" stainless steel coupler. We bored the coupler to allow a 1/8" outer diameter molybdenum feed tube to be inserted fully through the coupler and into the cathode tube, ensuring that liquid zinc did not contact the stainless steel coupler. We sealed the feed tube to the coupler with a graphite ferrule to ensure that the diameter of the feed tube was not affected by swaging. We wrapped a stainless steel coaxial heater around the entire coupler such that the zinc was evaporated inside this section. To ensure the heat was contained to this section, we retained the coaxial heater inside a steel retaining tube and wrapped it in multi-layer insulation (MLI). We inserted a thermocouple between the coupler and the heater to facilitate active temperature control. This assembly is labeled "boost heater" in Fig. 1a for its use to 'boost' downstream temperatures to above zinc's melting point.

Behind the coupler/boost heater section, we placed an aluminum block heater for the purpose of melting the propellant. The aluminum block contained a slot for a thermocouple, a hole for the feed tube, and a slot for a steel cartridge heater. This heater is labeled "liquidus heater" in Fig. 1a for its use to maintain the liquidus temperature of the zinc wire. With this heater we aimed to establish a consistent melting point for the wire, utilizing the boost heater to guarantee liquid/vapor states downstream of the liquidus heater and relying on passive cooling to maintain a solid state upstream of the liquidus heater. Both the boost and liquidus heaters were actively controlled so as to be resilient to fluctuations in emitter temperature.

The zinc wire was fed into the cathode at the back end of the feed tube by means of a stepper motor-driven gear system adapted from a 3D printer extruder. Because we utilized commercially available extruder parts (for which 1.75 mm is a standard filament size), the smallest zinc wire diameter we could accommodate was 1.5 mm. We interfaced the feed tube to the extruder with a coupler that threaded directly into the stepper motor housing and retained the feed tube via set screws, as shown in Fig. 1a. We also used these set screw attachment points as the electrical connection points for the cathode power line.

To perform active temperature control, we used an Arduino inside the test chamber to regulate the power to the boost and liquidus heaters (we continuously drove the HCHT500ST heater to ensure a minimum emission temperature at the emitter). The Arduino read thermocouple temperatures via a pair of Adafruit AD8495 thermocouple amplifiers. To modulate the average heater power, the Arduino employed a PID controller to vary the duty cycle of a pulse-width-modulation (PWM) signal sent to an optical relay which delivered power to the boost and liquidus heaters.

B. Facility

We performed our experiments in the University of Michigan Plasmadynamics and Electric Propulsion Laboratory's Cathode Test Facility (CTF). Figure 2 shows a notional top view diagram of CTF with the experiment apparatus installed. CTF measures 0.6 m in diameter by 1 m long and is pumped by a 135 CFM scroll pump and a 20" CVI TM500 cryopump with a measured pumping speed of 1500 L/s on Xe. A gate valve separates the cryosail from the main test environment, enabling rapid venting/re-pumpdown cycles. To minimize zinc contamination of the facility walls and cryosail, we lined the chamber with aluminum foil and installed a pair of angled aluminum plates (chevrons) in front of the gate valve. We anticipated that zinc would condense on these sacrificial surfaces which could be cleaned and/or replaced as needed. To measure pressure, we used an InstruTech IGM401 Hornet ion gauge mounted at the wall of the test facility through a 90° elbow. During this campaign the chamber achieved a base pressure of $\sim 2 \times 10^{-6}$ Torr on air. At 10 sccm of krypton flow, the chamber pressure was $\sim 2 \times 10^{-4}$ Torr. At 10 sccm of zinc flow, the chamber typically measured $\sim 1.2 \times 10^{-5}$ Torr. This order of magnitude difference highlights the advantage of condensable propellants for ground testing.

We delivered electrical power to a cylindrical anode by means of a TDK-Lambda GEN 50-300 power supply operating in current-controlled mode. The TDK power supply reports current to one decimal place of precision and voltage to two decimal places. We verified the anode-to-cathode potential with a calibrated Fluke multimeter and found the voltages to be consistent within 0.2V. Because we manually recorded only one data point at each operating condition (after a short settling time), we do not report uncertainties in current or voltage.

C. Diagnostics

1. Langmuir probes

To measure plasma properties, we obtained Langmuir probe measurements using a Keithley 2400 source meter. During the first zinc test we employed a cylindrical Langmuir probe measuring 4.65 mm long by 0.46 mm diameter. During the second zinc test and all krypton testing, we employed a cylindrical probe measuring 5.92 mm long by

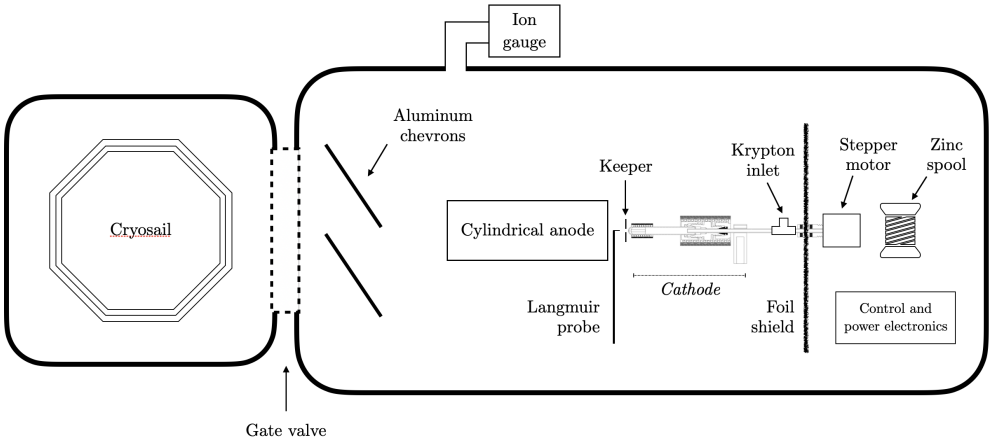

Fig. 2 Schematic top view of the experimental configuration.

0.25 mm diameter. In all tests, the tip of the probe was located 3.5 mm downstream of the cathode tip in front of an anode located 16 mm downstream, as shown in Fig. 3a. We used the Langmuir probes to obtain measurements of the plasma potential, plasma density, and electron temperature in the cathode plume using standard techniques for electric propulsion per Lobbia and Beal [14] except for the use of the 'kneedle' algorithm [15] to obtain the plasma potential. Figure 3 shows an example analysis of a Langmuir probe trace taken at 10 sccm krypton flow, 15 A discharge current.

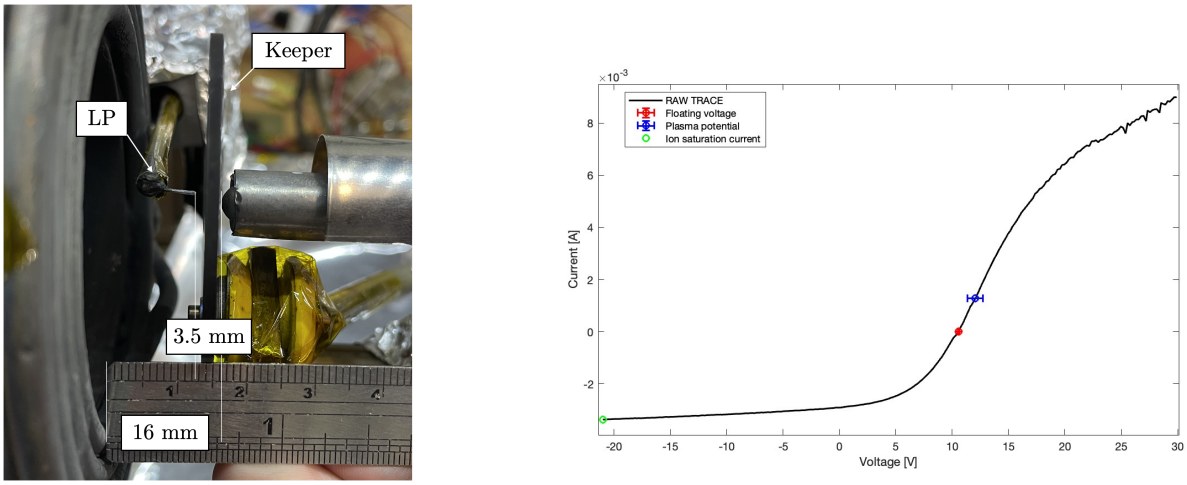

(a) **(b)**

Fig. 3 (a) Experimental placement of Langmuir probe in the cathode assembly and (b) example of Langmuir probe trace for a 10 sccm Kr, 15 A discharge with plasma potential labeled.

2. Time-resolved current measurement

To characterize oscillations, we employed a Keysight MSOX3054G oscilloscope to measure anode oscillations by means of a Pearson coil attached immediately downstream of the positive output line of the power supply. We recorded oscillation data for a duration of 20 ms at a sample rate of 3.125×10^6 Hz. To obtain smoother measurements, we split the full recording into ten equally sized samples (i.e. 2 ms) in the time domain, performed a fast Fourier transform over each sample, and computed the frequency-wise mean across all ten samples. An example sample-averaged power spectrum overlaid upon a full-recording power spectrum is shown in Fig. 4. We show here the mean power value as a solid line inside a filled band. The top and bottom of the band correspond to the 80th percentile of the time-domain

samples. Given the sample length and Nyquist frequency, the resolvable frequency spectrum was 500 Hz to 1.56×10^6 Hz.

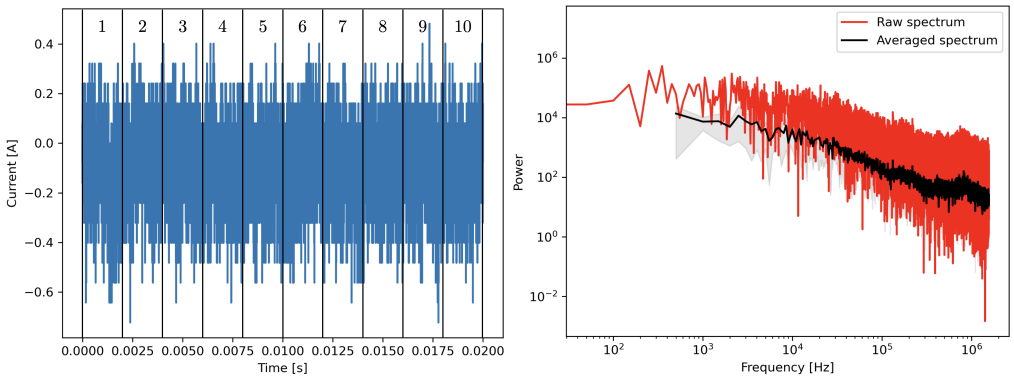

(a) **(b)**

Fig. 4 (a) Example raw oscillation with ten-sub sample slicing and (b) corresponding averaged power spectrum over the ten slices for the operating condition of 10 sccm Kr, 15 A discharge current.

D. Operating conditions

We collected zinc data across two tests (hereafter referred to as Test 1 and Test 2) and krypton during a single test between the two zinc tests. Table 1 shows a summary of the operating conditions and telemetry we investigated in this work. In zinc Test 1, we collected anode I-V characteristic and Langmuir probe measurements at anode currents of 8-20A and flow rates of 10 and 15 sccm. We primarily used Test 1 to characterize the thermal control system and did not collect oscillation data during this test. Figure 5a is a photograph of the cathode running on zinc during Test 1.

	Zn Test 1	**Kr Test**	**Zn Test 2**
Flow rate [sccm]	10, 15	5, 10, 15	10
Anode current [A]	8-16	10-30	15-25
Langmuir probe [in]	0.183×0.018	0.233×0.010	Saturated
Anode current oscillations	None	All points	Four points

Table 1 Summary of data collected between the three tests.

In the single krypton test, we collected anode I-V measurements at anode currents of 10-30A and flow rates of 5, 10, and 15 sccm. Out of concern for zinc condensation on the Langmuir probe following Test 1 changing the effective collection area of the probe, we replaced the probe prior to the krypton test. Figure 5b is a photograph of the cathode running on krypton during this test.

In zinc Test 2, we collected anode I-V measurements at anode currents of 15-25A and a flow rate of 10 sccm. Here the same Langmuir probe used in the krypton test consistently exceeded the source meter supply current before reaching electron saturation, so we obtained no useful Langmuir probe measurements. During Test 2 we recorded anode current oscillations, but due to instabilities in the thermal control system we only obtained these measurements at four operating conditions.

III. Results

In this section, we report the results of testing our cathode on krypton and zinc propellants under the operating conditions described in Sec. II.D.

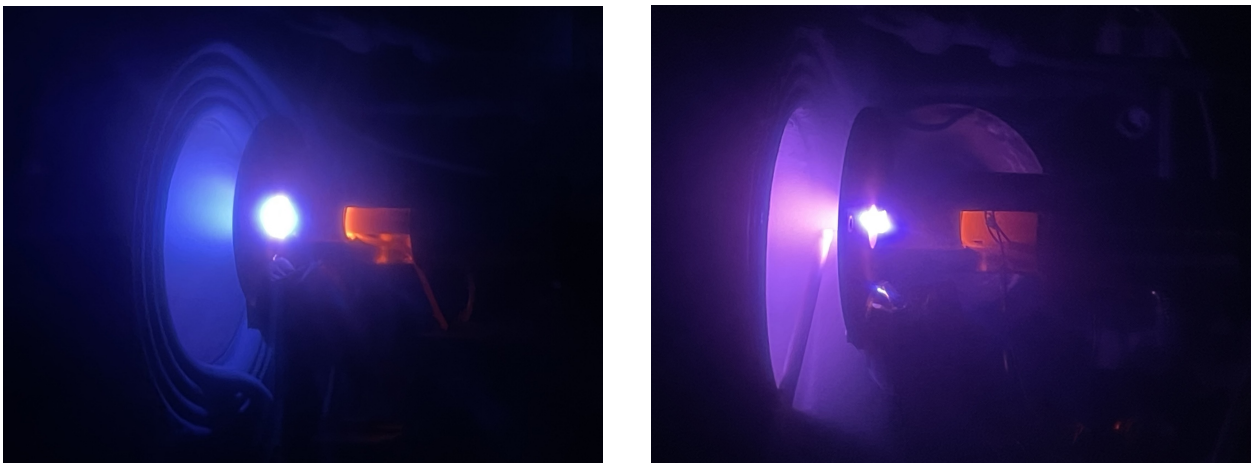

(a) **(b)**

Fig. 5 Photographs of the cathode operating (a) on zinc during Test 1 and (b) on krypton.

A. Current-voltage characteristics

In Test 1 we performed an I-V trace with zinc across 8-16 A of anode current with a settling time of 1-2 mins between points and repeated this sweep three times. These traces are shown in color in Figs. 6a and were taken in the following sequence:

- We allowed the cathode to thermally equilibrate at a steady-state operating condition of 11 A, 8.44 V.
- We recorded data while advancing the current from 11 to 16 A (shown in blue in Fig. 6a).
- We recorded data while decreasing the current from 16 to 8 A (shown in solid red in Fig. 6a).
- We immediately ramped the current from 8 to 16 A and recorded data while decreasing current until the cathode extinguished at 10 A (shown in dotted red in Fig. 6a).

We attribute the minor hysteresis of these curves to thermal effects, a process we discuss further in Sec. IV. With that said, across all three traces, we observe the coupling voltage decrease, reach a minimum, and then increase again. This is consistent with previous findings of hollow cathode I-V characteristics [16, 17]. We attribute the negative slope at low currents to the resistivity of the plasma decreasing as the number of charge carriers increases; once the resistance of the plasma is sufficiently low, the resistance of the circuit (e.g. the electrical lines) and near-field plasma dominate, and the voltage exhibits a positive slope.

In Test 2, we swept the anode current from 15-25A with zinc and allowed a settling time of 5-7 minutes between points to allow a thermocouple attached to the cathode tube behind the emitter to reach thermal steady state. This trace is shown in black in Fig. 6a.

For krypton, we recorded I-V data at currents of 10-30 A for 10 sccm flow with a settling time of 1-2 mins between points. Figure 6b shows the krypton I-V characteristic data plotted alongside the zinc characteristic data. It is notable that the coupling voltage required to extract a given current is roughly half for zinc as compared to krypton, suggesting the zinc plasma exhibits a lower resistivity than the krypton plasma. We discuss a possible origin for this in Sec. IV.

Figure 6c shows I-V characteristics for krypton and zinc at 15 sccm of flow. The zinc data were taken during Test 1 per the following procedure:

- We raised the flow rate from 10 to 15 sccm and allowed the cathode to thermally equilibrate at a 9.15V/15 A discharge.
- We dropped the current to 10 A and allowed the discharge to settle for 1 minute.
- We recorded data while advancing the current from 10 to 20 A with 1-2 minute settling times.

The shape of these curves are also broadly consistent with results on previous cathodes at moderate flow rates [17, 18].

B. Plasma properties

We extracted plasma potential, electron temperature, and ion number density from Langmuir probe measurements taken during zinc Test 1 and the krypton test following best practices established in [14]. Figure 7 shows the plasma properties for 10 and 15 sccm of flow.

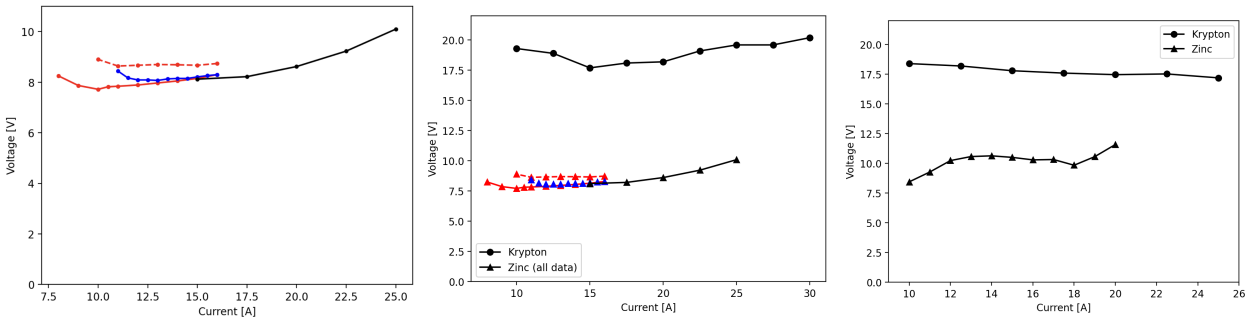

(a) (b) (c)

Fig. 6 Current-voltage characteristics at 10 sccm of flow. (a) Test 1 sweeps of 11-16 A (blue), 16-8 A (solid red), and 16-10 A (dotted red) alongside Test 2 (black). (b) Krypton characteristics plotted alongside the zinc characteristics shown in 6a. (c) Current-voltage characteristics at 15 sccm of flow for zinc (Test 1) and krypton.

As shown in Fig. 7a, the plasma potential mirrors the trends in discharge voltage for both propellants (Fig. 6b) as a function of discharge current. The magnitude of the potential for both propellants and flow rates are lower than the discharge values. This reflects the fact that there is a monotonic increase in plasma potential from the cathode to the anode, and the probe is located at an intermediate location in this potential rise. Notably, as was the case with the discharge voltage, the local plasma potential for zinc is lower than the krypton case, indicating qualitatively a lower effective resistance in the near-field plume from cathode body to anode.

Figure 7b shows the electron temperature as a function of discharge current in the plume. The magnitude of these values are broadly similar with previous measurements of cathodes operating on krypton and xenon [19–21] at this range of discharge currents. There is in both cases and flow rates a moderate increase with current, which is qualitatively consistent with the interpretation that higher currents drive increased Ohmic heating [22]. With that said, we note that the temperatures with zinc propellant are lower by nearly a factor of two compared to the krypton case for the 10 sccm flow rate. This in turn may be a reflection of reduced Ohmic heating for the zinc case, which is in observation in keeping with our conclusion from the measurements of plasma potential and discharge voltage that plasma resistance is lower with zinc. The temperature gap between propellants closes at higher flow rates (within experimental uncertainty).

Fig. 7c shows a comparison of the plasma density as a function of discharge current for both propellants. This result indicates again a weak dependence on current for both propellants with current, which may be indicative of enhanced ionization arising from higher Ohmic heating. Consistent as well with our other results, the higher plasma density would correspond to reduced resistivity in the plume for the zinc propellant case. As with the electron temperature results, however, we note that the gap between densities with zinc and krypton closes at higher flow rates.

In summary, the combination of experimental measurements of plasma properties and potential broadly indicate that operation of the cathode on zinc is in family with cathode operation on a noble gas at comparable operating conditions. There are minor departures in the near field properties, suggesting a potentially lower effective plasma resistance with this gas. We discuss in Sec. IV possible physical processes that may drive this.

C. Oscillations

We show in Fig. 8 a comparison of the power spectra in the discharge current at three operating conditions during Test 2 (15, 17.5 and 22.5 A of anode current), all at a flow rate of 10 sccm. In these results, the solid line corresponds to the mean of the ten power spectra while the shaded regions correspond to the 80th percentile of the ten power spectra at each frequency. As can be seen, in comparing these results to previous studies [23], the krypton spectra are broadly consistent with previous experimental characterization of oscillations in these devices. They are broadband and incoherent with a minor peak in the 10s of kHz range. This peak historically has been associated with an ionization-like instability. In contrast, the zinc spectra are virtually flat at high frequencies with a minor peak also approximately in the 10-100 kHz range. The magnitude of this oscillation is nearly an order of magnitude lower than the oscillation exhibited by the krypton case. Physically, this comparison thus reveals that while the zinc propellant may have qualitatively similar low frequency oscillations, the discharge overall appears to be more quiescent for these operating conditions. We return to a discussion of this result in the following section.

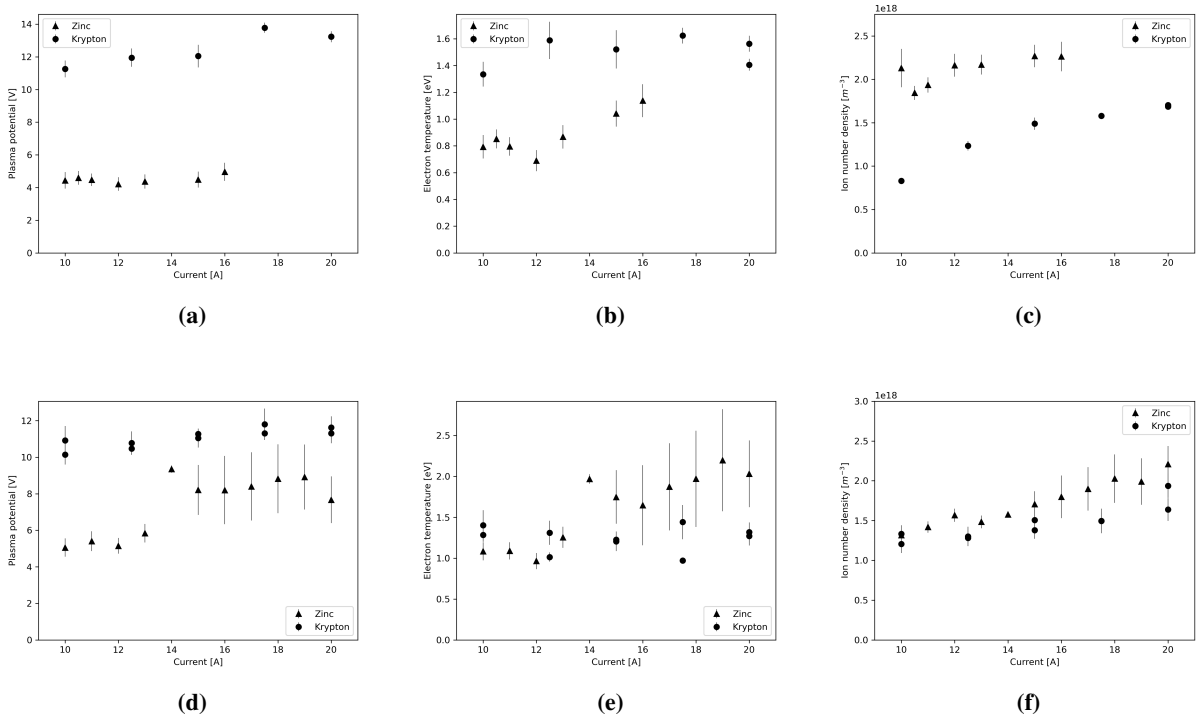

Fig. 7 Comparison of plasma properties for zinc and krypton discharges at 10 sccm flow showing (a) Plasma potential vs. anode current, (b) Electron temperature vs. anode current, and (c) Ion density vs. anode current. Comparison at 15 sccm flow showing (d) Plasma potential vs. anode current, (e) Electron temperature vs. anode current, and (f) Ion density vs. anode current.

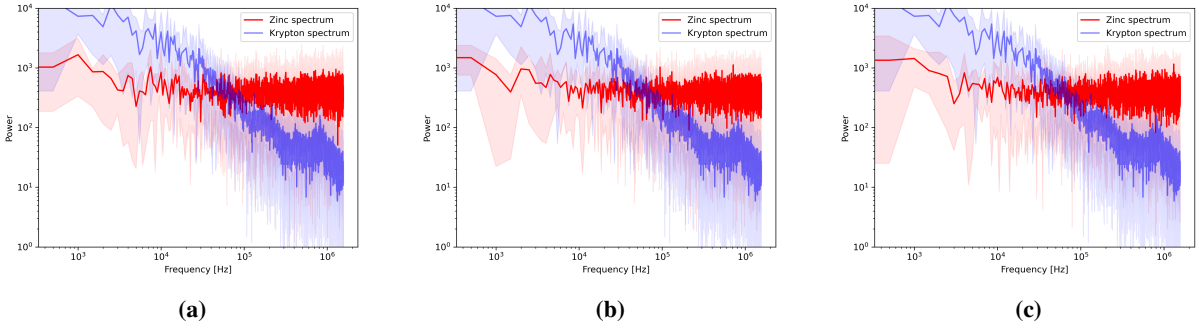

Fig. 8 Anode current oscillations at 10 sccm of flow for (a) 15.0 A anode current, (b) 17.5 A anode current, and (c) 22.5 A anode current.

IV. Discussion

We discuss in this section key comparisons on the plasma properties, global operation, and oscillations of the hollow cathode operating on zinc and krypton. We first draw attention to hysteretic behavior in the IV traces. We then examine possible explanations for the major differences in coupling voltage and oscillation spectra.

A. Thermal effect on I-V characteristics

Figure 6a shows that the repeated I-V characteristics in zinc Test 1 varied in local minimum shape and vertical offset. During Test 1, we recorded these measurements serially (i.e. continuously, with 1-2 mins of settling time between data points) in the order shown in Fig. 9. We began by allowing the cathode to thermally equilibrate at a steady-state operating condition of 11 A, 8.44 V (Fig. 9 point 1). We then proceeded to advance the current to a peak 16 A (point 2) and decrease the current to a minimum 8 A (point 3). We immediately ramped the current to 16 A (point 4) and decreased it again until the cathode extinguished at 10 A (point 5).

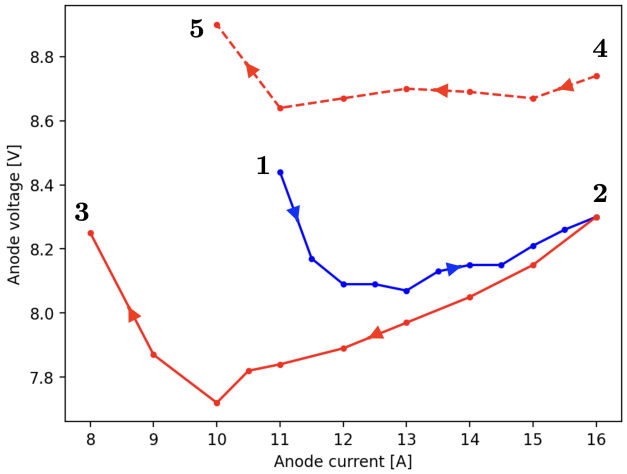

Fig. 9 Sequence in which I-V data were collected during zinc Test 1.

We attribute the cathode's variable performance to variations in temperature as a result of raising and lowering the discharge power. Unlike noble gas cathodes which employ an active mass flow controller, the zinc cathode flow rate varies during the settling period due to the fact that higher discharge powers induce higher temperatures upstream in the flow tube indeed the change from point 2 to point 3 results in a 50% drop in the cathode power; this, we believe, induces evaporation of the advancing zinc wire farther upstream, momentarily allowing a higher flow rate to occur. During temperature monitoring in Test 2, we observed the temperature settling time of upstream cathode components to be ~5-7 mins, rather than the 1-2 mins used in Test 1. As a result, Test 1 was susceptible to thermally-induced fluctuations in zinc flow rate. The behavior observed in Fig. 9 could therefore be explained as follows:

1) The cathode begins at thermal steady state and increases in temperature during measurements 1 → 2.
2) Excessive propellant evaporation improves performance (i.e. lower anode voltages and minimum current level) during measurements 2 → 3 and evaporates wire further upstream.
3) Continual cooling during measurements 2 → 3 causes the evaporation front to move downstream into a region where the zinc wire is now depleted.
4) Measurements 4 → 5 take place with an artificially low propellant flow rate, thereby inducing lower performance over the initial I-V sweep, 1 → 2.

We note that this theory is consistent with behavior observed by Makela et al. [9], who remarked that increasing the discharge power of a zinc propellant Hall thruster drove higher anode temperatures and therefore evaporation rates at their consumable zinc anode. For our constant wire feed rate system, this behavior implies that increasing the discharge power of our system will trigger a flow rate-induced performance transient caused by excess wire evaporation. This transient will be arrested when the wire/evaporation front reaches a new thermal equilibrium.

B. Lower plasma resistance with zinc

As we have discussed in the preceding, the lower discharge voltages (Figs. 6b, 6c), plasma potentials (Figs. 7a, 7d), and temperatures (Figs. 7b, 7e) in all suggest qualitatively that the effective plasma resistance of the cathode plume is lower in the case of zinc compared to krypton. This physically can be understood from a consideration of the effective resistivity in the near field which scales as

$$\eta = \frac{m_e \nu_c}{q^2 n_e}, \tag{1}$$

where m_e is the electron mass, ν_c is the effective electron collision frequency for electrons, q is fundamental charge, and n_e is the local plasma density. In practice, the effective resistance of mid-current cathode plumes has been shown to be driven in large part by non-classical effects such as the onset of ion-acoustic turbulence [23–25]. This stems from the strong electron current driven in these devices. It has been demonstrated in previous work that an approximate form for this collision frequency, per the so-called Sagdeev scaling, scales with the plasma frequency (i.e. $\nu_c \propto \omega_{pe}$) [26]. If this is indeed the case for our system, we would expect the ratio of plasma resistivities in the near field to follow

$$\frac{\eta_{\mathrm{Zn}}}{\eta_{\mathrm{Kr}}} = \left(\frac{n_{e(Kr)}}{n_{e(Zn)}}\right)^{1/2}. \tag{2}$$

This would suggest qualitatively that the driving factor in resistance for the cathode coupling is the plasma density. We have shown (Figs. 7c, 7f) that the near field plasma density for zinc propellant is higher; this result may in part explain the trends in other plasma properties and over the discharge voltage we observe at the 10 sccm case. Notably, we see that as the densities become comparable at the 15 sccm case, the disparities in temperature and plasma potential close, further lending credence to the role of plasma density in driving these effects.

With this result in mind, this begs the question ultimately as to why the plasma densities are higher with the zinc propellant. To first order, this result is unexpected given that zinc is a smaller molecular with a lower effective cross-section for ionization. There are a number of conflating factors, however, that we are not able to directly assess experimentally. For example, the internal temperature and pressures inside the cathode may be fundamentally different for the two gases–a result of the differences in injection schemes and vapor pressure of the flow. If the pressures are higher in the case of zinc, for example, this would result in higher effective ionization rates, despite the cross-section. Evaluating these causes is beyond the scope of the present investigation, but we point out that in practice, the differences in behavior are not marked. Despite the fundamentally different propellants, the overall resistances, temperatures, and densities do not differ more than a factor of two.

C. Oscillations

As we briefly outlined in the discussion of oscillations (Fig. 8) in the cathode plume, the operation of the system on zinc is notably more quiescent–particularly at lower frequencies—than the case with krypton. The nature of low frequency oscillations in these discharges remains an open area of investigation, so it is not possible to conclusively point to a first-principles underlying cause for this discrepancy.

With that said, it has been suggested [25] that the presence of non-classical resistivity in the plume may be a driver for the onset of lower frequency oscillations. Given that our estimates for resistivity suggest that zinc exhibits a lower effective electron impedance, the conditions may be not satisfied for strong growth. In practice, however, we again remark that although the spectra have different magnitudes, the response of the cathode plasma to zinc are not outside the expected family for noble gas plasmas.

V. Conclusion

In summary, metal-propellant electric propulsion systems enable high power operation on the ground due to their condensability and in space due to their high storage densities and low costs. Historically, condensible propellants have been delivered to laboratory thrusters by sublimation or boiling, but these systems struggle with propellant metering and are difficult to scale for high power flight operation. To overcome these problems, we built and tested a wire feed system to deliver zinc propellant to a BaO hollow cathode and compared the performance of the cathode on zinc and krypton.

Our test article comprised a COTS hollow cathode tip on a custom body assembly and utilized multiple stages of heaters to control the melting and vaporization of a zinc wire. We outfitted the U-M Cathode Test Facility to accommodate a condensible propellant and observed background pressures during zinc operation that were an order of magnitude lower than on krypton, highlighting the key advantage of condensible propellants for ground testing. We

obtained anode I-V characteristics, plume Langmuir probe measurements, and oscillation measurements for 10 and 15 sccm of flow.

In the I-V characteristics, we observed coupling voltages that were approximately 50% lower for zinc than for krypton. We attribute this lower coupling voltage to a lower plasma resistivity for zinc. We also recorded oscillations in the anode current for zinc and krypton. We showed that while the zinc discharge is more quiescent, the oscillatory nature of the plume of the zinc plasma is in family with other discharges.

This work demonstrates the use of wire feeding as a means of delivering a metal propellant and the feasibility of operating a BaO cathode on zinc propellant. It highlights the advantage of condensability on facility background pressure and identifies how a higher power efficiency in the form of lower coupling voltages may be attained with alternative propellants. It also demonstrates a wire feed system that does not rely on gravity and enables propellant to be precisely metered without thermal runaway and evaporated without heating the entire propellant reservoir. This overcomes previous condensible propellant feed system limitations and provides a proof of concept for a flight-like method of metal propellant delivery. Ultimately, this work identifies a path forward for enhancing high-power electric propulsion testing on Earth and scaling in space.

Acknowledgements

This work was supported by the DARPA Thruster Advancements for Low-altitude Operations in Space (TALOS) research program and by the National Science Foundation Graduate Research Fellowship Program (NSF GRFP).

References

[1] Närger, U., and Balzarini, D. A., "Coexistence-curve diameter and critical density of xenon," *Physical Review B*, Vol. 42, No. 10, 1990, p. 6651.

[2] Marrese-Reading, C., Sengupta, A., Frisbee, R., Polk, J., Cappelli, M., Boyd, I., Keidar, M., Tverdokhlebov, S., Semenkin, S., Markusic, T., et al., "The VHITAL program to demonstrate the performance and lifetime of a bismuth-fueled very high Isp Hall thruster," *41st AIAA/ASME/SAE/ASEE Joint Propulsion Conference & Exhibit*, 2005, p. 4564.

[3] Tverdokhlebov, O. S., and Semenkin, A., "An overview of the TSNIIMASH/TSE efforts under VHITAL program," *29th International Electric Propulsion Conference*, 2005.

[4] Sengupta, A., Marrese-Reading, C., Semenkin, A., Zakharenkov, L., Tverdokhlebov, S., Tverdokhlebov, O., Polzin, K., Markusic, T., Cappelli, M., Scharfe, D., et al., "Summary of the VHITAL Thruster Technology Demonstration Program A Two-Stage Bismuth-Fed Very High Specific Impulse TAL," *Proceedings of 30th International Electric Propulsion Conference*, 2007, pp. 1–11.

[5] Polzin, K., Markusic, T., Stanojev, B., and Marrese-Reading, C., "Integrated liquid bismuth propellant feed system," *42nd AIAA/ASME/SAE/ASEE Joint Propulsion Conference & Exhibit*, 2006, p. 4636.

[6] Szabo, J., Robin, M., and Hruby, V., "Bismuth vapor Hall Effect Thruster performance and plume experiments," *The 35th International Electric Propulsion Conference, Atlanta, Georgia*, 2017, pp. 10–8.

[7] Massey, D., King, L., and Makela, J., "Development of a direct evaporation bismuth Hall thruster," *44th AIAA/ASME/SAE/ASEE Joint Propulsion Conference & Exhibit*, 2008, p. 4520.

[8] Szabo, J., Robin, M., Duggan, J., and Hofer, R. R., "Light metal propellant Hall thrusters," *31st International Electric Propulsion Conference*, 2009, pp. 2009–138.

[9] Makela, J. M., Washeleski, R. L., Massey, D. R., King, L. B., and Hopkins, M. A., "Development of a magnesium and zinc Hall-effect thruster," *Journal of Propulsion and Power*, Vol. 26, No. 5, 2010, pp. 1029–1035.

[10] Tirila, V.-G., Ryan, C., Demaire, A., and Hallock, A., "Performance investigation of zinc propellant in sub kw class hall thrusters," 2022.

[11] Barrow, M., Tirila, V.-g., Dworski, S., and Ryan, C., "Development of a 2.2 kw hall thruster operating on zinc or magnesium as the propellant," *39th International Electric Propulsion Conference*, 2025.

[12] Makela, J., Massey, D., and King, L., "Performance Characteristics of a LaB6 Bismuth Cathode for use with Hall Thrusters," *42nd AIAA/ASME/SAE/ASEE Joint Propulsion Conference & Exhibit*, 2006, p. 4634.

[13] Makela, J. M., Massey, D. R., and King, L. B., "Bismuth hollow cathode for Hall thrusters," *Journal of Propulsion and Power*, Vol. 24, No. 1, 2008, pp. 142–146.

[14] Lobbia, R. B., and Beal, B. E., "Recommended practice for use of Langmuir probes in electric propulsion testing," *Journal of Propulsion and Power*, Vol. 33, No. 3, 2017, pp. 566–581.

[15] Satopaa, V., Albrecht, J., Irwin, D., and Raghavan, B., "Finding a" kneedle" in a haystack: Detecting knee points in system behavior," *2011 31st international conference on distributed computing systems workshops*, IEEE, 2011, pp. 166–171.

[16] Dodson, C. A., Perez-Grande, D., Jorns, B. A., Goebel, D. M., and Wirz, R. E., "Ion heating measurements on the centerline of a high-current hollow cathode plume," *Journal of Propulsion and Power*, Vol. 34, No. 5, 2018, pp. 1225–1234.

[17] Csiky, G., "Measurements of Some Properties of a Discharge From a Hollow Cathode," Tech. Rep. NASA TN D-4966, NASA Lewis Research Center, Cleveland, OH, Feb. 1969.

[18] Philip, C., "A study of hollow cathode discharge characteristics," *Aiaa Journal*, Vol. 9, No. 11, 1971, pp. 2191–2196.

[19] Goebel, D. M., Jameson, K. K., Watkins, R. M., Katz, I., and Mikellides, I. G., "Hollow cathode theory and experiment. I. Plasma characterization using fast miniature scanning probes," *Journal of Applied Physics*, Vol. 98, No. 11, 2005.

[20] Suazo Betancourt, J. L., Butler-Craig, N., Lopez-Uricoechea, J., Bak, J., Lee, D., Steinberg, A. M., and Walker, M. L., "Thomson scattering measurements in the krypton plume of a lanthanum hexaboride hollow cathode in a large vacuum test facility," *Journal of Applied Physics*, Vol. 135, No. 8, 2024.

[21] Roberts, P., Brown, Z., and Jorns, B., "Hollow cathode electron properties are consistent with marginally stable turbulence," *Applied Physics Letters*, Vol. 126, No. 7, 2025.

[22] Polk, J., Goebel, D., Watkins, R., Jameson, K., and Yoneshige, L., "Characterization of hollow cathode performance and thermal behavior," *42nd AIAA/ASME/SAE/ASEE Joint Propulsion Conference & Exhibit*, 2006, p. 5150.

[23] Goebel, D. M., Becatti, G., Mikellides, I. G., and Lopez Ortega, A., "Plasma hollow cathodes," *Journal of Applied Physics*, Vol. 130, No. 5, 2021.

[24] Jorns, B. A., Mikellides, I. G., and Goebel, D. M., "Ion acoustic turbulence in a 100-A LaB 6 hollow cathode," *Physical Review E*, Vol. 90, No. 6, 2014, p. 063106.

[25] Georgin, M. P., Jorns, B. A., and Gallimore, A. D., "Transient non-classical transport in the hollow cathode plume I: measurements of time-varying electron collision frequency," *Plasma Sources Science and Technology*, Vol. 29, No. 10, 2020, p. 105010.

[26] Ortega, A. L., Jorns, B. A., and Mikellides, I. G., "Hollow cathode simulations with a first-principles model of ion-acoustic anomalous resistivity," *Journal of Propulsion and Power*, Vol. 34, No. 4, 2018, pp. 1026–1038.